Screening adsorbent-working solution pairs for adsorption-driven osmotic heat engines based on experimental water adsorption isotherm database and machine learning

Yanan Zhao [1], Zhilu Liu [1], Mingliang Li, Rui Long [*], Song Li [*], Zhichun Liu, Wei Liu

School of energy and power engineering, Huazhong University of Science and Technology, Wuhan 430074, PR China

ABSTRACT

Osmotic heat engines have attracted increasing attention in harvesting ultra-low temperature waste heat. In order to fill the gap in the high-throughput computational screening of adsorbent-aqueous salt solution working pairs for adsorption-driven osmotic heat engines, an experimental water adsorption isotherm database is constructed and eight common salt-water solutions are selected to identify the high-performance work pairs with system energy efficiency as evaluation indicator. The relationship between adsorbent properties, adsorbent structure characteristics and system performance is systematically analyzed. Results revealed that high working capacity and moderate adsorption enthalpy of adsorbents and large osmotic coefficients of salts are beneficial to energy efficiency. Adsorbents with larger accessible surface area, moderate available pore volume and critical pore diameter are favorable. Furthermore, regression machine learning is employed for achieving fast and accurate prediction of the system energy efficiency to accelerate screening. Genetic algorithm is adopted to search for the best-performing working pair properties.

1. Introduction

Low-temperature waste heat widely exists in the industrial processes (Kumar and Rakshit, 2021; Farhat et al., 2022). It is estimated that 72% of primary energy is eventually discharged into environment as waste heat due to the inefficient thermodynamic process (Forman et al., 2016). The recovery and utilization of waste heat contributes to energy saving, reducing energy consumption and alleviating environmental issues. Traditional thermodynamic systems such as organic Rankine cycle and Kalina cycle have been wildly developed to recover low-grade heat (Long et al., 2019; Arslan and Yılmaz, 2022; Köse et al., 2022). However, their performance is not satisfactory when operating at ultra-low temperature below 80 ℃. Recently, osmotic heat engines (OHEs) were proposed to provide technical solutions for exploiting such waste heat.

Osmotic heat engines aiming at converting low-grade heat into electricity usually consist of two main units, one is the regeneration unit devoted to thermally separating the salt solution into high and low concentration solutions, as well as restoring the initial concentration of the working solution, the other is the power generation unit for capturing the salinity gradient produced in the regeneration unit and converting the Gibbs free energy of mixing into electricity (Lin et al., 2014). Common technologies employed in regeneration unit include membrane distillation (MD) (Zaragoza et al., 2014), multiple effect distillation (MED) (Hu et al., 2019) and adsorption-based desalination (AD) (Wu et al., 2010; Li et al., 2021). In the power generation unit, the most promising technologies recognized are pressure retarded osmosis (PRO) (Tedesco et al., 2015; Long et al., 2018a) and reverse electrodialysis (RED) (Long et al., 2018a, 2018b; Lacey, 1980).

Efforts have been devoted to emphasizing configuration design and operation condition optimization of osmotic heat engine. Ortega-Delgado et al (Ortega-Delgado et al., 2019). conducted a comprehensive exergy analysis of a RED-MED heat engine and the effects of the main operation and design variables on the exergy efficiency were assessed, the result shows that a maximum exergy efficiency of 24% can be obtained when operating under working concentration of 4.5–0.01 mol/L and solutions velocity of 0.2–0.36 cm/s with high-performing membranes. Long et al (Long et al., 2017). proposed an osmotic heat engine combined MD and RED, and an electrical efficiency of 1.15% is

---

achieved when operating between 60 ℃ and 20 ℃ with 5 mol/kg NaCl as working solution. Hu et al (Hu et al., 2018). performed a thermodynamic analysis of a MED-RED hybrid system to investigate the effect of operation and structure parameters on system performance, the result indicated that an energy conversion efficiency of 0.85% can be obtained with heat source temperature of 95 ℃ and working concentration of 3.75 mol/kg. Zhao et al (Zhao et al., 2020a). proposed an AD-PRO for power and cooling cogeneration, the electricity generation as well as refrigeration performance of the system were theoretically evaluated, the effects of operational conditions were also analyzed. Results indicated a maximum exergy efficiency of 33.9% under a waste heat temperature of 50 ℃. A further study by Zhao et al (Zhao et al., 2020b). explored the dynamic response of an AD-RED heat engine through dynamic modeling the power and cooling cogeneration system, an exergy efficiency of 30.14% was obtained at desorption time of 900 s and switching time of 10 s with CAU-10 as adsorbent. The potential applications of osmotic heat engines have also been evaluated in latest studies. Tong et al (Tong et al., 2020). investigated the feasibility of the thermolytic osmotic heat engine with NH_4HCO_3 solution as working fluid to harvest industrial waste heat, and it was found that an energy return on investment value of approximately 55 can be obtained, which indicates the suitability of using industrial waste heat to generate electricity. Zhao et al (Zhao et al., 2021). presented an advanced osmotic heat engine combined AD and RED and carried out a practical simulation of the small-scale OHE harvesting solar energy for electricity generation, a largest average electric power of 41.8 W and a highest electric efficiency of 1.04% were achieved. Catrini et al (Catrini et al., 2021). conducted a prospective analysis on integrating the osmotic heat engine into cogeneration plants, and the benefits of energy, economy and environment were obtained by proposing two different applications and investigating three illustrative case studies.

In the regeneration unit, AD has become a competitive candidate due to its superior thermal separation capability at ultra-low temperature, low electricity consumption, and simple process (Olkis et al., 2019, 2018). Adsorbent-solution working pairs play a decisive role in the adsorption process, hence screening suitable combinations of adsorbent and working solution is critical for system performance optimization. Various adsorbent-solution working pairs for adsorption systems (e.g. AD and adsorption heat pumps) were investigated (Li et al., 2020). Vasta et al (Vasta et al., 2012). tested a prototype of an adsorption-driven mobile air conditioner with zeolite-water pair and an attractive coefficient of performance (COP) of around 0.4 is returned. Pan et al (Pan et al., 2019). designed and manufactured an adsorption air-conditioner employing silica gel-water working pair to experimentally investigated the performance under various conditions, and a cooling power of 3.98 kW and COP of 0.632 were reached. Metal–organic frameworks (MOFs) regarded as the most promising adsorbents are also extensively investigated. Given the increasing number of MOFs, high-throughput computational screening (HTCS) based on grand canonical Monte Carlo (GCMC) simulations is widely adopted to efficiently evaluate the performance of MOF-alcohol (methanol and ethanol) working pairs (Li et al., 2017; Ahmed et al., 2019). Erdos et al (Erdos et al., 2018). computationally screened 2930 experimentally synthesized MOFs on the basis of the working capacity calculated from GCMC simulations for adsorption heat pumps with methanol and ethanol as working fluids. Long et al (Long et al., 2021a). carried out a HTCS of 1322 computationally ready MOFs based on GCMC simulations for AD-PRO heat engine with LiCl-methanol solution as working fluid. Different from alcohols, it is difficult to computationally screen MOF-water working pairs via GCMC simulations due to the extremely high computational cost of simulating water adsorption (Colón and Snurr, 2014). To address the challenge of screening high-performance adsorbent-water working pairs from a vast number of adsorbents, Liu et al (Liu et al., 2021). for the first time conducted the HTCS of adsorbent-water working pairs for adsorption-driven heat pumps instead of carrying out GCMC of water adsorption. They calculated system performance by constructing a

database containing the water adsorption isotherms of over 231 adsorbents and establishing a mathematical model of the thermodynamic system. However, the high-throughput computational screening of adsorbent-aqueous salt solution working pairs for adsorption-based osmotic heat engine has not been implemented so far.

As shown in Fig. 1, in this study, we construct an experimental water adsorption isotherm database including 311 kinds of adsorbents and selected eight common salts to identify the high-performance work pairs which can lead to high efficiency for adsorption-reversed electrodialysis heat engine. The relationship between adsorbent properties, adsorbent structure characteristics and system performance is systematically analyzed. Regression machine learning for predicting system energy efficiency via main working pair properties collected from the database is conducted to accelerate the screening of adsorbent-aqueous salt solution working pairs. Genetic algorithm is adopted to search for the best-performing working pair properties with the energy efficiency as the optimization objective. This study performs the high-throughput computational screening of adsorbent-aqueous salt solution working pairs for adsorption-driven heat engines and may provide guidance for designing high-performance novel adsorbents for adsorption-based OHEs. This study could also provide efficient methods to explore potential adsorbents for water harvesting from air, adsorption heat pumps, dehumidification and desalination.

2. Adsorption-driven osmotic heat engine

As shown in Fig. 2, the adsorption-driven osmotic heat engine consists of an adsorption-based desalination unit for thermally separating the salt solution into high concentration and low concentration solutions and a reverse electrodialysis unit for directly converting the Gibbs free energy of the mixture of two solutions produced in AD unit into electricity. The ideal thermodynamic process of AD is composed of four steps, as shown in Fig. 3. The solvent water first evaporates from the evaporator at ambient temperature and the evaporated water vapor is then absorbed by the adsorbent at the constant evaporation pressure with an external cooling water circuit removing the sorption heat. Low-grade heat is put into the system for preheating meanwhile elevating the pressure to condensation pressure. Then the solvent is desorbed from the surface of the adsorbent in an isobaric desorption process driven by low-grade heat and condensed into pure water in the condenser, thereby producing high and low concentration solutions. Afterward, the adsorption bed is precooled for the next adsorption. The produced high and low concentration solutions are subsequently charged into the RED unit and the salinity gradient between them drives the ions transport through the membranes. In the RED stack, cation exchange membranes (CEMs) and anion exchange membranes (AEMs) are alternatively arranged, which regulate the movement direction of cations and anions, resulting in a net ionic current. Finally, the net ionic current is converted to electrical current via redox reactions on the electrodes.

In this work, the thermodynamic process of AD is considered to be ideal and the results are all normalized (Zhao et al., 2020a). Therefore, the parameters of the heat engine are independent. An updated experimental water adsorption isotherm database (EWAID 2.0) containing 311 adsorbents was constructed based on the original version of EWAID 1.0 including 231 adsorbents collected from NIST/ARPA-E Database. The detailed build process of EWAID 1.0 can be found in our previous work (Liu et al., 2021). In the updated EWAID 2.0, five MOFs from NIST/ARPA-E database and other adsorbents from the latest scientific literature were added. The data of 311 adsorbents including the source of literature and structural characteristics were provided in Table S1-S2. Here, 311 experimental water adsorption isotherms were fitted by the universal adsorption isotherm model (UAIM) applicable to various types of isotherms at different temperatures. The working capacity ΔW equals the difference of water uptake between adsorption and desorption obtained from isotherms predicted by UAIM as described as (Ng et al., 2017)
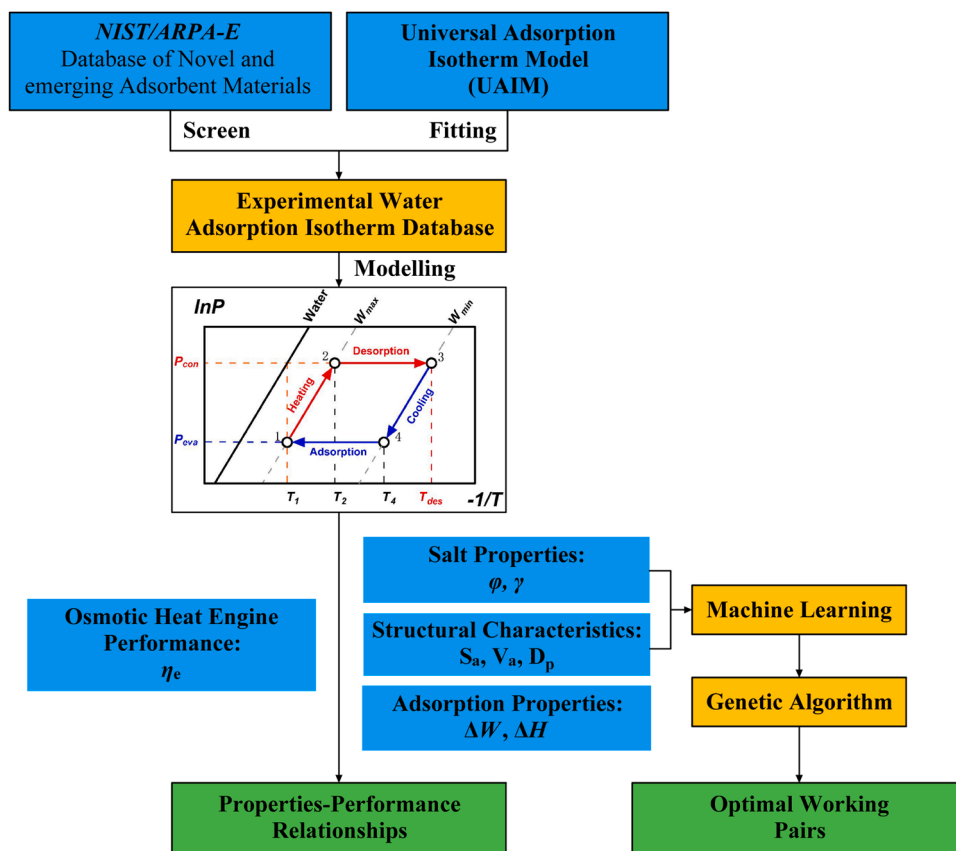
Fig. 1. Schematic diagram of the proposed computational screening approach for developing high performance adsorption-driven osmotic heat engine.
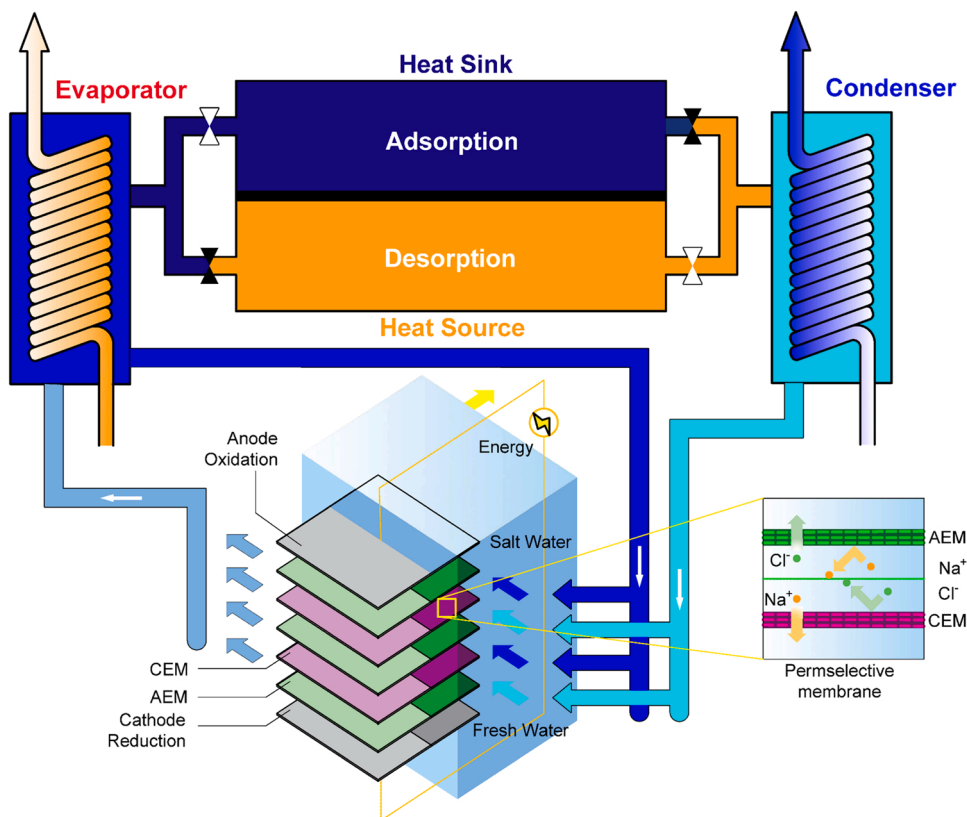

Fig. 2. Schematic diagram of the adsorption-reversed electrodialysis heat engine.
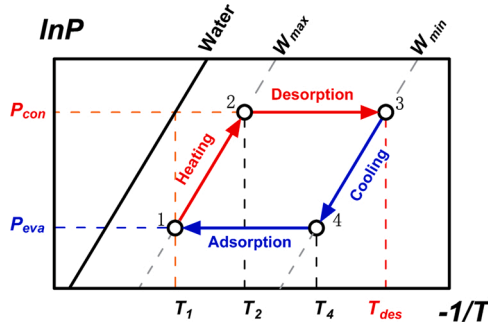
Fig. 3. Isosteric diagram of the ideal adsorption-based desalination process, including four steps of isobaric adsorption, isosteric heating, isobaric desorption and isosteric cooling.

$$W = \sum_{i=1}^{n} \alpha_i \left\{ \frac{\left(\frac{P}{P_0} \exp\left(\frac{\varepsilon_i}{RT}\right)\right)^{\frac{RT}{m_i}}}{1 + \left(\frac{P}{P_0} \exp\left(\frac{\varepsilon_i}{RT}\right)\right)^{\frac{RT}{m_i}}} \right\}_i \quad (1)$$

where W is the water equilibrium uptake, P and T represent the equilibrium pressure and temperature, and P_0 is the saturation pressure of water, R is the universal gas constant. Additionally, α_i, ε_i, m_i and n are the fitting parameters determined by the characteristic of adsorption isotherms. Therefore, the working capacity of the adsorbent can be obtained by

$$\Delta W = W_{max} - W_{min} = W(T_{ads}, P_{ev}) - W(T_{des}, P_{con}) \quad (2)$$

The enthalpy of adsorption ($\Delta_{ads}H$) is calculated using the predicted adsorption isotherms at varying temperatures according to the Clausius-Clapeyron equation (Ramirez et al., 2005)

$$\Delta_{ads}H = -R \frac{\partial(\ln p)}{\partial(1/T)} \quad (3)$$

The average enthalpy of adsorption ($\Delta_{ads}H_{ave}$) is the average value of isosteric heat of adsorption between W_{min} and W_{max}, which can be estimated as

$$\Delta_{ads}H_{ave} = \frac{\int_{W_{min}}^{W_{max}} \Delta_{ads}H(W)dW}{W_{max} - W_{min}} \approx \frac{\Delta_{ads}H(W_{max}) + \Delta_{ads}H(W_{min})}{2} \quad (4)$$

The total regenerative heat Q_{reg} consists of two parts. Before the desorption process, heat Q_{1-2} is required for isosteric heating to elevate the pressure to the saturation pressure at the condensing temperature, then heat Q_{2-3} is required for isobaric heating during the desorption process (Supplemental Information). The specific energy consumption (SEC) indicating the heat required per kilogram of water vapor desorbed can be described as (Wu et al., 2012)

$$SEC = \frac{Q_{reg}}{m_{sb}\Delta W} \quad (5)$$

The Gibbs free energy of mixing is adopted to evaluate the theoretical maximum work extracted in the RED process. The molar Gibbs free energy of mixing is defined as (Yip and Elimelech, 2012)

$$-\Delta G_{mix} = RT \left\{ \left[\sum x_i \ln(\gamma_i x_i) \right]_M - \Lambda_A \left[\sum x_i \ln(\gamma_i x_i) \right]_A - \left[\Lambda_B \sum x_i \ln(\gamma_i x_i) \right]_B \right\} \quad (6)$$

where x and γ denote the mole fraction and activity coefficient, respectively. The subscripts A, B and M indicate solution A, solution B, and mixture of the two solutions. Λ is the molar fraction of each solution in the final mixture, thus $\Lambda_A + \Lambda_B = 1$. At low concentrations, the mole fraction and activity coefficient of water can be approximated to a value of 1, then it is assumed that the total volume is constant during mixing process due to the negligible effect of the mole and volume of salt

compared to water. Hence the Gibbs free energy of mixing ΔG_{mix} can be approximated as (Yip and Elimelech, 2012)

$$-\frac{\Delta G_{mix}}{\nu RT} \approx c_M \ln(\gamma_{s,M} c_M) - \Psi c_{low} \ln(\gamma_{s,low} c_{low}) - \left(1 - \Psi\right) c_{high} \ln(\gamma_{s,high} c_{high}) \quad (7)$$

where ν is the total dissociated ions number and $\Psi \approx V_{low}/(V_{low} + V_{high})$. The activity coefficient γ is given by the Pitzer correlations (Pitzer and Mayorga, 1973), which can can be found in Supplemental Information.

To improve the energy efficiency of the osmotic heat engine, heat recovery is considered in this study and solid porous matrix regenerator is adopted for compensating the heat needed in desorption process (Long et al., 2021b). It is assumed that the temperature of the regenerator T_r is uniform and the heat capacity is huge. The heat recovery from the cooling water at outlet is calculated as $Q_{r,c} = m_c c_{p,c}(T_{des} - T_r)$ and the heat can be reused is calculated as $Q_{r,h} = m_h c_{p,h}(T_r - T_1)$, where the subscripts c and h denote the cooling and heating process, respectively. Therefore, the net regeneration heat needed can be expressed as $Q_{reg,net} = Q_{reg} - Q_{r,h} = Q_{reg} - m_h c_{p,h}(T_r - T_1)$ and it is indicated that larger T_r brings higher energy efficiency according to the equation. Due to $Q_{r,c} \geq Q_{r,h}$ in an actual process, temperature of the regenerator meets the relation of $T_r \leq \frac{T_{des} + \omega T_1}{1 + \omega}$, where $\omega = \frac{m_h c_{p,h}}{m_c c_{p,c}}$ denotes the asymmetric heat specific ratio. The maximum $T_r = \frac{T_{des} + T_1}{2}$ is achieved when the cooling medium is the same as the heating medium during the heat recovery process, which indicates about 50% heat carried by cooling water is recovered.

Hence the maximum theoretical energy efficiency considering heat recovery can be finally calculated as

$$\eta_e = \frac{\Delta G_{mix}}{Q_{reg} - m_h c_{p,h}(T_{des} - T_1)/2} \quad (8)$$

3. Results and discussion

In order to to identify the high-performance work pairs which can lead to high efficiency for adsorption-reversed electrodialysis heat engine, we constructed an experimental water adsorption isotherm database including 311 kinds of adsorbents collected from NIST/ARPA-E Database of Novel and Emerging Adsorbent Materials ($author1$ et al., 42] </id>) and the latest scientific literature. The adsorbents are classified into five species, including carbon, covalent-organic frameworks (COFs), metal-organic frameworks (MOFs), porous organic polymers (POPs) and zeolites. In addition, the structural properties of most adsorbents in the database including accessible surface area (S_a), available pore volume (V_a) and pore diameter (D_p) were also collected from the literature. The source literature of adsorbents and detailed structural characteristics can be found in Table S1-S2. The adsorption properties of each adsorbent under eight kinds of working salts (i.e. MgI_2, $MgBr_2$, LiCl, $LiNO_3$, NaCl, KBr, $NaNO_3$ and $AgNO_3$) and the corresponding energy efficiency of the system were also computed. The evaporation and condensation temperatures are set to be the same as the ambient temperature of 293 K and the desorption temperature is set at 333 K. The detailed operational conditions of the adsorption-driven osmotic heat engine are listed in Table S3.

3.1. System performance of adsorbent-aqueous salt solution working pairs

As shown in Figs. 4 and 5, the distribution of system electric efficiency under different adsorbent species for divalent and univalent working aqueous salt solutions are presented. The horizontal lines correspond to the five species of adsorbents mentioned above and the vertical axis correspond to the efficiency of the adsorption-driven osmotic heat engine. The distribution of system electric efficiency corresponding to various adsorbents with different SEC is illustrated by boxplot graphs. The electric efficiency of most adsorbents for divalent
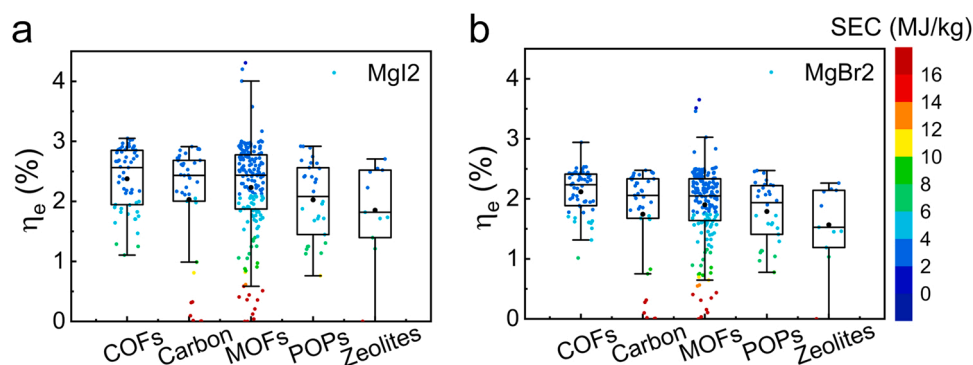
Fig. 4. Distribution of system electric efficiency colored by specific energy consumption under different adsorbent species for divalent salt solutions.
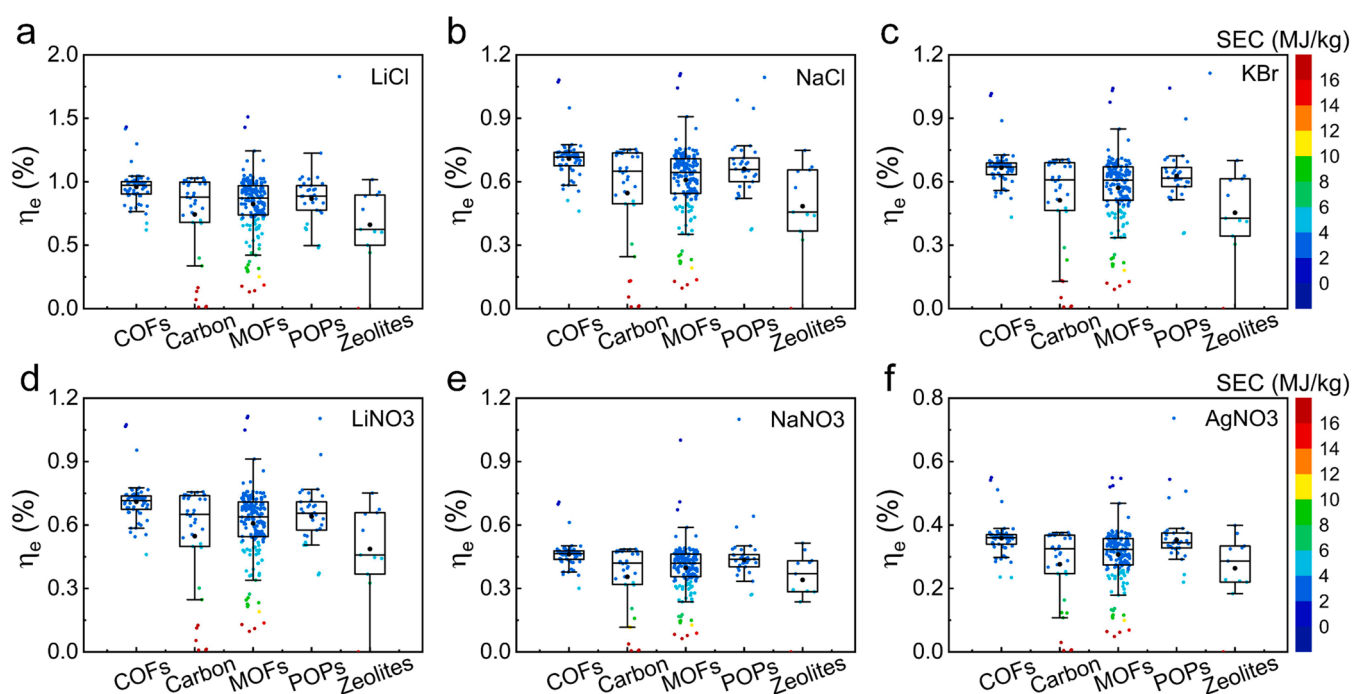

Fig. 5. Distribution of system electric efficiency colored by specific energy consumption under different adsorbent species for univalent salt solutions.

Table 1
Top 10 identified combinations of salt and adsorbent with the highest electric efficiency.

Ranking	Adsorbents	Species	Metal type	Salts	η_e (%)	ΔW (g/g)	ΔH (MJ/kg)	S_a (m²/g)	V_a (cm³/g)	D_p (Å)
1	S-MIL-53(Al)	MOF	Al	MgI₂	4.308	0.319	1.777	n.d.	n.d.	n.d.
2	MIL-125	MOF	Ti	MgI₂	4.201	0.263	1.799	1510	0.68	n.d.
3	MIL-101-NH₂	MOF	Cr	MgI₂	4.004	0.905	2.006	2509	1.27	34[c2]
4	S-MIL-53(Al)	MOF	Al	MgBr₂	3.650	0.358	1.762	n.d.	n.d.	n.d.
5	{[Cu₂(4pmpmd)₂(CH₃OH)₄(opd)₂] * 2 H₂O}	MOF	Cu	MgI₂	3.577	0.121	1.971	n.d.	n.d.	6.48[c2]
6	MIL-125	MOF	Ti	MgBr₂	3.513	0.268	1.799	1510	0.68	n.d.
7	MIL-101-NH₂	MOF	Cr	MgBr₂	3.461	0.935	1.936	2509	1.27	34[c2]
8	Cr-MIL(101)	MOF	Cr	MgI₂	3.169	0.623	2.537	3124	1.58	34[c2]
9	Tp-Azo	COF	–	MgI₂	3.051	0.063	2.067	942	n.d.	27[c1]
10	TpBpy	COF	–	MgI₂	3.0286	0.614	2.661	2336	n.d.	24.2[c1]

n.d. represents "no data".
For S_a: [a] Langmuir surface area; no superscript represents BET surface area.
For V_a: [b1] pore volume measured basing on H₂O adosrption; [b2] pore volume measured using mercury intrusion method; no superscript default is based on N₂ adsorption.
For D_p: [c1] average pore diameter; [c2] largest cavity diameter; [c3] dominant pore size obtained according to pore size distribution.

salt varies between 1% and 3%, while for univalent salt, the electric efficiency is relatively small and varies between 0% and 1%, which can be attributed to the more number of ions of divalent salt than that of monovalent salt under a certain working concentration, resulting in larger Gibbs free energy. It can be found that the adsorbents corresponding to the maximum efficiency are all MOFs, and COFs render the best average performance regardless of the type of working salts. The best performance adsorbents for various salts are COFs. For divalent salt, MOFs perform better than carbon, POPs and Zeolites, while for univalent salt, POPs perform better than MOF, carbon and Zeolites. More than 50% of COFs displayed an electric efficiency of over 2.5% with MgI₂ as working salt, and around 75% of COFs exhibited an electric efficiency higher than 2%. It is also noticed that SEC has a strictly negative correlation with the electric efficiency under all operational conditions.

The top 10 combinations of working salt and adsorbent with the highest electric efficiency are listed in Table 1. Best-performing adsorbents with the highest efficiency for each working salt are also summarized in Table S4. It was found that almost all adsorbents with the best performance are MOF and COF. Among all the combinations, adsorption-based osmotic heat engine with S-MIL-53(Al) as adsorbent and MgI₂ as working salt can achieve the maximum electric efficiency of 4.308%. The adsorbent S-MIL-53(Al) has wide applicability for the adsorption of various salts, and the efficiency achieved by its combination with almost all salts ranks the top five among all adsorbents.

3.2. Relationship between adsorbent properties and system performance

Working capacity and adsorption enthalpy are two important properties of the adsorbent. Working capacity indicated the mass of solvent absorbed by unit mass of adsorbent, which can be calculated as the difference between the maximum and minimum uptake of the adsorbents. In the adsorption process, a larger working capacity means a better separation of salt solution and thereby elevating the work extracted in power generation unit. According to equation (S10), adsorption enthalpy significantly correlated with the regeneration heat. The relationship between adsorbent properties and system energy efficiency is depicted in Fig. 6, where 8 kinds of working salts are employed. There is an obvious positive correlation between working capacity and energy efficiency under a certain working solution. For divalent salts, the energy efficiency of the system increases significantly with the increase of the working capacity when ΔW is less than 0.3 g/g, while there is no significant enhancement in efficiency when ΔW is larger, and for univalent salts, the specific ΔW is 0.2 g/g. In addition, neither higher nor lower adsorption enthalpy leads to best efficiency, adsorbents with moderate adsorption enthalpy (1.8–2.6 MJ/kg in this study) exhibit more favorable performance for each working aqueous salt solution. It can also be found that, in general, the osmotic coefficient of working salt
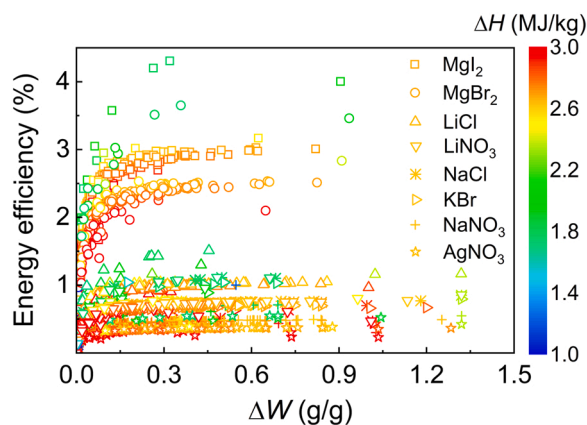
is generally positively correlated with the energy efficiency of system. As shown in Fig. 7a, divalent salts possess much larger osmotic coefficients than univalent salts, resulting in higher energy efficiency as a whole. Among the 8 kinds of salts, MgI₂ with the largest osmotic coefficient leads to the best system performance, while AgNO₃ is opposite.

3.3. Relationship between adsorbent structure characteristics and system performance

The structural characteristics of the adsorbents in the database including accessible surface area (S_a), available pore volume (V_a) and pore diameter (D_p) were collected from scientific literature to investigate the relationship between adsorbent structure characteristics and system performance. Fig. 8(a-c) demonstrates that the adsorption behavior of the adsorbents is strongly correlated with the structure characteristics. There exsits an obvious positive relationship between adsorption capacity and S_a. The adsorption capacity increases with increasing V_a, up to a maximum at around 1.5 cm³/g then decreases due to weakened interaction between water and adsorbents at a large V_a. The working capacity also generally exhibits a trend of first increasing and then decreasing with the increase of diameter, reaching a peak value at the pore diameter of around 24 Å. This can be attributed to that continuous reversible adsorption occurs in pores with a D_p larger than water dynamic diameter of 2.7 Å and smaller than a certain critical diameter, while when D_p is larger than the critical diameter, undesirable thermodynamic irreversible capillary condensation will occur (de Lange et al., 2015). The critical diameter can be calculated as $D_c = 4\sigma T_c/(T_c - T)$, where σ is the approximate water molecule size (0.28 nm), T_c and T are the critical and actual temperature of water, thus the critical diameter under ambient temperature can be obtained as around 21 Å (Liu et al., 2021; Benoit et al., 2013). Given that the number of experimental water adsorption isotherms in the database collected from previous literature is limited, the data corresponding to the pore diameter of around 21 Å is insufficient, therefore, the theoretical maximum working capacity under the critical diameter is not observed. In summary, the structure-performance relationship showed that adsorbents with higher surface area (S_a > 1500 m²/g), medium available pore volume (V_a ~1.5 cm³/g) and pore diameter (D_p ~24 Å) showed higher working capacity and energy efficiency. The structural characteristics of top MOFs are consistent with the structure-performance relationship we obtained, and the preferred metal type of high-performing MOFs are Al, Cr Ti and Cu as seen in Table 1and Table S4. It is also noticed that salts with lower osmotic coefficient lead to larger working capacity when the structural characteristics of the adsorbent are constant. This can be attributed to that high osmotic coefficient results in low evaporation pressure, that is, adsorption pressure, as depicted in Fig. 7, thereby reducing the maximum uptake at the end of the adsorption process, and the minimum uptake at the end of the desorption process is related to the condensation pressure and independent of the working salt, as shown in Fig. 9. The relationship between system energy efficiency and adsorbent structure characteristics is presented in Fig. 8(d-f). For divalent salts, the energy efficiencies exhibit significant increase with the increase of the three structure characteristic parameters under smaller S_a, V_a and D_p due to the elevated working capacity, then the working capacity exceeded 0.3 g/g, resulting in unobvious change in energy efficiency. In addition, the energy efficiency decreases due to the reduced working capacity when the pore diameter is larger than the critical diameter. For univalent salts, the effect of characteristic parameters on energy efficiency is not as significant as that on divalent salt due to the relatively high working capacity of the adsorbents for univalent salts, which is mostly greater than the specific ΔW of 0.2 g/g.

3.4. Machine learning and optimization

Due to the high precision, flexibility and convenient scalability, machine learning has been widely used in many fields, such as fault
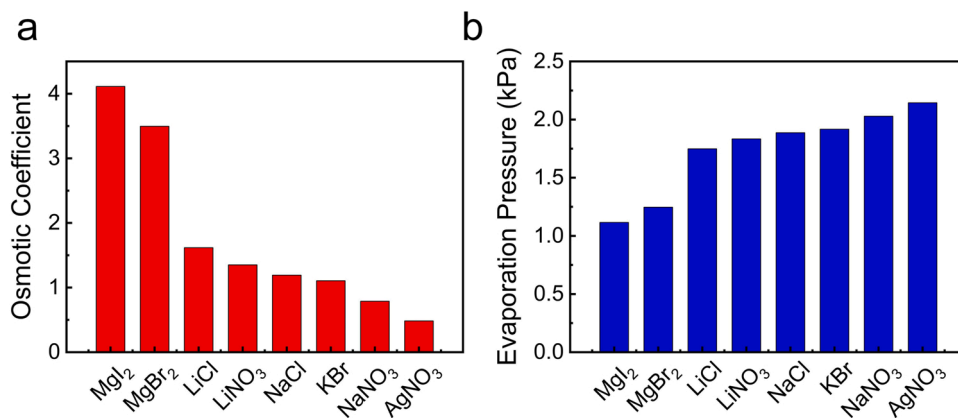

Fig. 6. The system energy efficiency of various adsorbents as a function of working capacity colored by adsorption enthalpy.

Fig. 7. Osmotic coefficient (a) and evaporation pressure (b) of 8 kinds of working aqueous salt solutions.
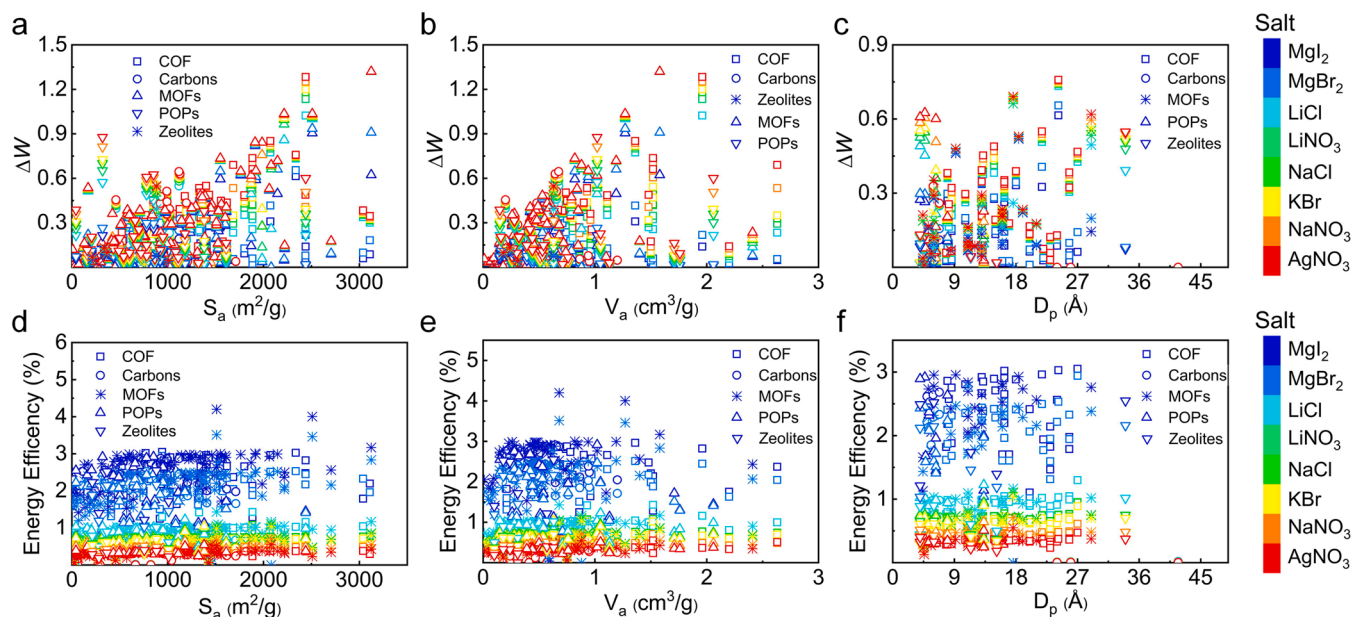

Fig. 8. The relationship between system working capacity energy efficiency (a-c) as well as energy efficiency (d-f) and adsorbent structure characteristics, including accessible surface area (S_a), available pore volume (V_a) and pore diameter (D_p).
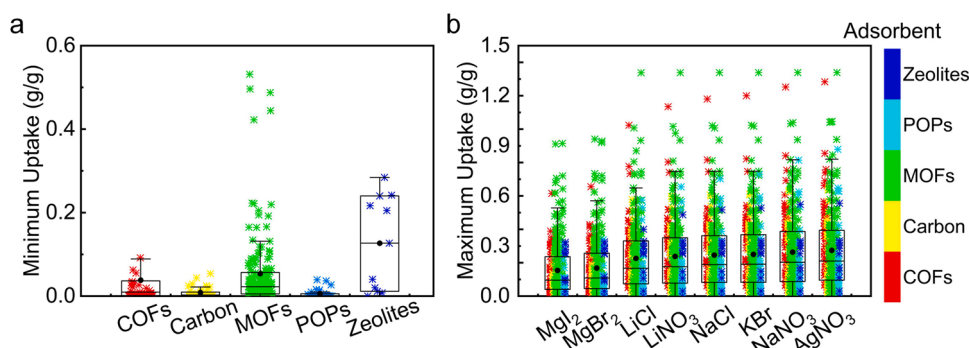

Fig. 9. The minimum uptake (a) and the maximum uptake (b) under different adsorbent and salt species.

diagnosis (Glowacz, 2021a, 2021b) and property prediction of energetic materials (Tian et al., 2022). In order to screen adsorbent-aqueous salt solution working pairs more efficiently, regression machine learning for finding the functional relationship to associate working pairs properties and system energy efficiency through training data collected in the

database is conducted. The main properties of working pairs are accessible surface area, available pore volume and pore diameter of the adsorbents as well as osmotic coefficient and activity coefficient of the salts. Here, we tried out four different candidates of regression machine learning models for predicting energy efficiency as shown in Fig. 10,
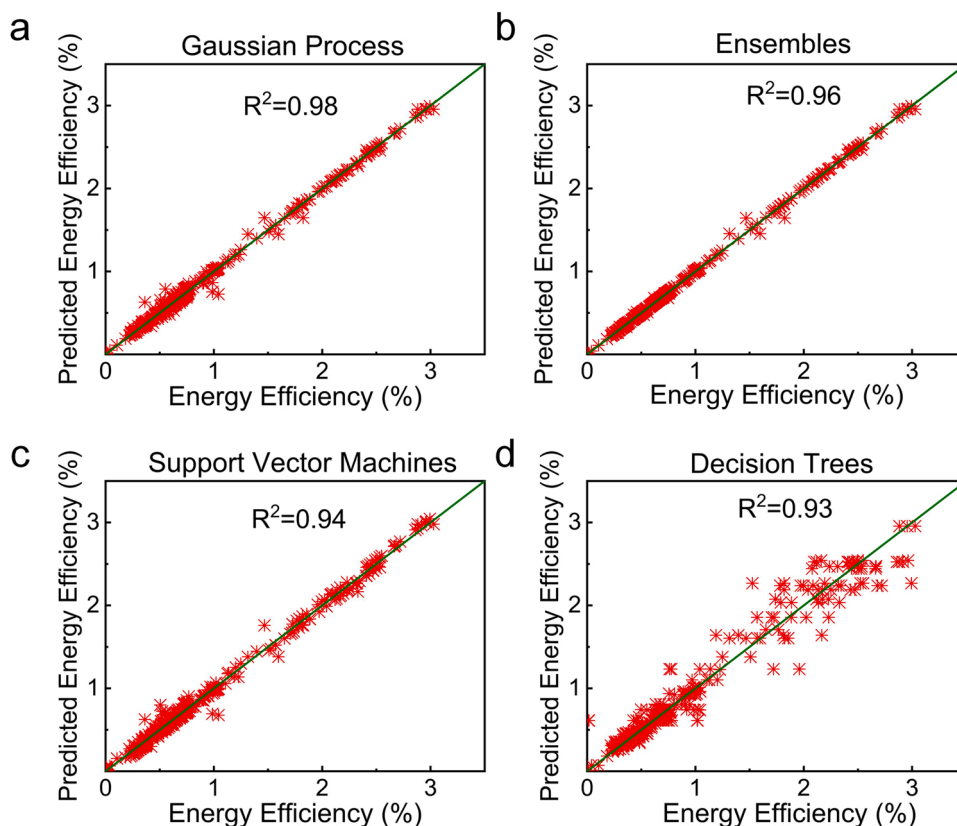
Fig. 10. Energy efficiency of the system predicted by 4 kinds of regression machine learning models.

whose hyper-parameters are automatically adjusted based on the Bayesian optimization. Indicators of root mean square error (RMSE), R-Squared (R^2), mean absolute error (MAE), mean square error (MSE) are used to evaluate the accuracy of the models, and their values for each model are displayed in Table S5 (Supplemental Information). In addition, 776 kinds of working pairs with five property parameters are selected from the experimental water adsorption isotherm database, and eighty percent of the data is randomly chosen for training the model while the remaining data is used for validation. The training results indicate that the energy efficiency of the system can be predicted accurately with the five property parameters of working pairs and Gaussian process model exhibits the highest accuracy with $R^2 = 0.98$, followed by the ensemble-based regression model with $R^2 = 0.96$, the support vector machines model with $R^2 = 0.94$ and the decision trees model with $R^2 = 0.87$.

Although machine learning is capable of making fast and relatively accurate prediction of the system energy efficiency based on the five job pair characteristics, it is still challenging for machine learning models to find the optimal solution in high-dimensional feature spaces (Jennings et al., 2019). Therefore, combined with the well-trained best performing Gaussian process model, the genetic algorithm is adopted to further search for the best-performing working pairs properties with the energy efficiency as the optimization objective. Fig. 11 shows the flowchart of the genetic algorithm optimization process and the initial population size is set at 5000. The optimal working pairs properties are the accessible surface area of 694.32 m^2/g, the available pore volume of 0.31 cm^3/g, the pore diameter of 9.22 Å, the osmotic coefficient of 5.04 and the activity coefficient of 3.96. The final energy efficiency after optimization is 4.25%, which is higher than all the efficiency predicted in machine learning and slightly lower than the maximum efficiency in the experimental water adsorption isotherm database due to the fitting errors of the regression model.
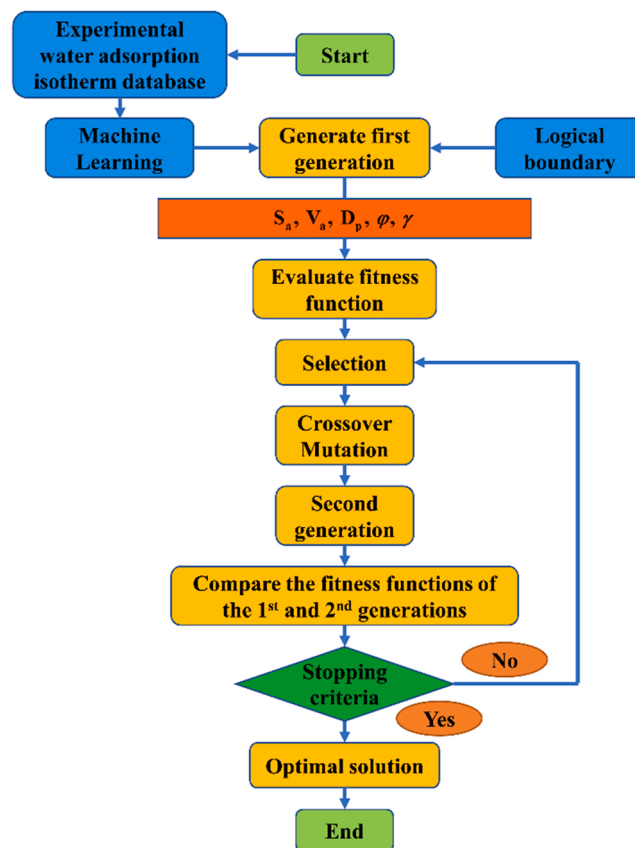

Fig. 11. The flowchart of the genetic algorithm optimization process.

4. Conclusions

In this study, we perform high-throughput computational screening of adsorbent-aqueous salt solution working pairs for adsorption-driven osmotic heat engine. An experimental water adsorption isotherm database including 311 kinds of adsorbents is constructed and eight common salts are selected to identify the high-performance adsorbent-aqueous salt solution work pairs. The relationships between properties of adsorbent-salt solution working pairs and performance of adsorption-driven osmotic heat engine is explored. Results show that MOFs exhibit the best performance for both divalent and univalent salts among the five species of adsorbents, and divalent salts render higher energy efficiency than univalent salts due to the larger Gibbs free energy of mixing. Specific energy consumption has a strictly negative correlation with electric efficiency. High working capacity and moderate adsorption enthalpy of adsorbents and large osmotic coefficients of salts are beneficial to energy efficiency. Adsorbents with larger accessible surface area, moderate available pore volume and critical pore diameter lead to higher working capacity thus the energy efficiency, and these three structural parameters have a more significant effect on the energy efficiency of divalent salts than univalent salts. In summary, high working capacity and moderate adsorption enthalpy of adsorbents and large osmotic coefficients of salts are beneficial to energy efficiency. Adsorbents with larger accessible surface area, moderate available pore volume and critical pore diameter are favorable. Regression machine learning for finding the functional relationship to associate working pairs properties (S_a, V_a, D_p, Φ and γ) and system energy efficiency through training data collected in the database is conducted. Moreover, genetic algorithm is adopted combined with the Gaussian process model well-trained via machine learning to further search for the best-performing working pair properties with energy efficiency as the optimization objective, and the final energy efficiency after optimization is 4.25%. This work offers a method of screening adsorbent-aqueous salt solution working pairs and provides guidance for designing high-performance novel adsorbents for adsorption-driven osmotic heat engines. In the next step, expanding the experimental water adsorption isotherms database is necessary for further exploration. In addition, the experimental validation of the screened adsorbents can also be conducted in the further work.

Declaration of Competing Interest

The authors declare that they have no known competing financial interests or personal relationships that could have appeared to influence the work reported in this paper.

Acknowledgements

Appendix A. Supporting information

Supplementary data associated with this article can be found in the online version at doi:10.1016/j.psep.2022.09.046.

References

Ahmed, A., Seth, S., Purewal, J., Wong-Foy, A.G., Veenstra, M., Matzger, A.J., et al., 2019. Exceptional hydrogen storage achieved by screening nearly half a million metal-organic frameworks. Nat. Commun. 10 (1), 1568.

Arslan, M., Yılmaz, C., 2022. Thermodynamic optimization and thermoeconomic evaluation of afyon biogas plant assisted by organic rankine cycle for waste heat recovery. Energy 248, 123487.

Benoit, Coasne, Anne, Galarneau, Roland, Pellenq, et al. Adsorption, intrusion and freezing in porous silica: the view from the nanoscale. Chemical Society Reviews. 2013.

Catrini, P., Cipollina, A., Micale, G., Piacentino, A., Tamburini, A., 2021. Potential applications of salinity gradient power-heat engines for recovering low-temperature waste heat in cogeneration plants. Energy Convers. Manag. 237, 114135.

Colón, Y.J., Snurr, R.Q., 2014. High-throughput computational screening of metal–organic frameworks. Chem. Soc. Rev. 43 (16), 5735–5749.

Erdos, M., de Lange, M., Kapteijn, F., Moultos, O., Vlugt, T., 2018. In silico screening of metal-organic frameworks for adsorption-driven heat pumps and chillers. ACS Appl. Mater. Interfaces 10.

Farhat, O., Faraj, J., Hachem, F., Castelain, C., Khaled, M., 2022. A recent review on waste heat recovery methodologies and applications: comprehensive review, critical analysis and potential recommendations. Clean. Eng. Technol. 6, 100387.

Forman, C., Muritala, I.K., Pardemann, R., Meyer, B., 2016. Estimating the global waste heat potential. Renew. Sustain. Energy Rev. 57, 1568–1579.

Glowacz, A., 2021a. Ventilation diagnosis of angle grinder using thermal imaging. Sensors 21 (8), 2853.

Glowacz, A., 2021b. Thermographic fault diagnosis of ventilation in BLDC motors. Sensors 21 (21), 7245.

Hu, J., Xu, S., Wu, X., Wu, D., Jin, D., Wang, P., et al., 2018. Theoretical simulation and evaluation for the performance of the hybrid multi-effect distillation—reverse electrodialysis power generation system. Desalination 443, 172–183.

Hu, J., Xu, S., Wu, X., Wu, D., Jin, D., Wang, P., et al., 2019. Exergy analysis for the multi-effect distillation - reverse electrodialysis heat engine. Desalination 467, 158–169.

Jennings, P.C., Lysgaard, S., Hummelshøj, J.S., Vegge, T., Bligaard, T., 2019. Genetic algorithms for computational materials discovery accelerated by machine learning. npj Comput. Mater. 5 (1), 46.

Köse, Ö., Koç, Y., Yağlı, H., 2022. Is Kalina cycle or organic Rankine cycle for industrial waste heat recovery applications? A detailed performance, economic and environment based comprehensive analysis. Process Saf. Environ. Prot. 163, 421–437.

Kumar, A., Rakshit, D., 2021. A critical review on waste heat recovery utilization with special focus on Organic Rankine Cycle applications. Clean. Eng. Technol. 5, 100292.

Lacey, R.E., 1980. Energy by reverse electrodialysis. Ocean Eng. 7 (1), 1–47.

de Lange, M.F., Verouden, K.J.F.M., Vlugt, T.J.H., Gascon, J., Kapteijn, F., 2015. Adsorption-driven heat pumps: the potential of metal–organic frameworks. Chem. Rev. 115 (22), 12205–12250.

Li, M., Zhao, Y., Long, R., Liu, Z., Liu, W., 2021. Gradient porosity distribution of adsorbent bed for efficient adsorption cooling. Int. J. Refrig. 128, 153–162.

Li, S., Chung, Y.G., Simon, C.M., Snurr, R.Q., 2017. High-throughput computational screening of multivariate metal–organic frameworks (MTV-MOFs) for CO$_2$ capture. J. Phys. Chem. Lett. 8 (24), 6135–6141.

Li, W., Xia, X., Li, S., 2020. Screening of covalent–organic frameworks for adsorption heat pumps. ACS Appl. Mater. Interfaces 12 (2), 3265–3273.

Lin, S., Yip, N.Y., Cath, T.Y., Osuji, C.O., Elimelech, M., 2014. Hybrid pressure retarded osmosis–membrane distillation system for power generation from low-grade heat: thermodynamic analysis and energy efficiency. Environ. Sci. Technol. 48 (9), 5306–5313.

Liu, Z., Li, W., Moghadam, P.Z., Li, S., 2021. Screening adsorbent–water adsorption heat pumps based on an experimental water adsorption isotherm database. Sustain. Energy Fuels 5 (4), 1075–1084.

Long, R., Li, B., Liu, Z., Liu, W.J.Joms, 2017. Hybrid membrane distillation-reverse electrodialysis electricity generation system to harvest low-grade thermal energy. J. Membr. Sci. 525, 107–115.

Long, R., Lai, X., Liu, Z., Liu, W., 2018a. A continuous concentration gradient flow electrical energy storage system based on reverse osmosis and pressure retarded osmosis. Energy 152, 896–905.

Long, R., Li, B., Liu, Z., Liu, W., 2018a. Reverse electrodialysis: modelling and performance analysis based on multi-objective optimization. Energy 151, 1–10.

Long, R., Li, B., Liu, Z., Liu, W., 2018b. Performance analysis of reverse electrodialysis stacks: channel geometry and flow rate optimization. Energy 158, 427–436.

Long, R., Kuang, Z., Li, B., Liu, Z., Liu, W.J.E.P., 2019. Exergy analysis and performance optimization of Kalina cycle system 11 (KCS-11) for low grade waste heat recovery. Energy Procedia 158, 1354–1359.

Long, R., Xia, X., Zhao, Y., Li, S., Liu, Z., Liu, W., 2021a. Screening metal-organic frameworks for adsorption-driven osmotic heat engines via grand canonical Monte Carlo simulations and machine learning. iScience 24 (1), 101914.

Long, R., Zhao, Y., Li, M., Pan, Y., Liu, Z., Liu, W., 2021b. Evaluations of adsorbents and salt-methanol solutions for low-grade heat driven osmotic heat engines. Energy 229, 120798.

Ng, K.C., Burhan, M., Shahzad, M.W., Ismail, A.B., 2017. A universal isotherm model to capture adsorption uptake and energy distribution of porous heterogeneous surface. Sci. Rep. 7 (1), 10634.

NIST/ARPA-E. Database of Novel and Emerging Adsorbent Materials.

Olkis, C., Santori, G., Brandani, S., 2018. An adsorption reverse electrodialysis system for the generation of electricity from low-grade heat. Appl. Energy 231, 222–234.

Olkis, C., Brandani, S., Santori, G., 2019. A small-scale adsorption desalinator. Energy Procedia 158, 1425–1430.

Ortega-Delgado, B., Giacalone, F., Catrini, P., Cipollina, A., Piacentino, A., Tamburini, A., et al., 2019. Reverse electrodialysis heat engine with multi-effect distillation: exergy analysis and perspectives. Energy Convers. Manag. 194, 140–159.

Pan, Q., Peng, J., Wang, H., Sun, H., Wang, R., 2019. Experimental investigation of an adsorption air-conditioner using silica gel-water working pair. Sol. Energy 185, 64–71.

Pitzer, K.S., Mayorga, G., 1973. Thermodynamics of electrolytes. II. Activity and osmotic coefficients for strong electrolytes with one or both ions univalent. J. Phys. Chem. 77 (19), 2300–2308.

Ramirez, D., Qi, S., Rood, M.J., Hay, K.J., 2005. Equilibrium and heat of adsorption for organic vapors and activated carbons. Environ. Sci. Technol. 39 (15), 5864–5871.

Tedesco, M., Cipollina, A., Tamburini, A., Bogle, I.D.L., Micale, G., 2015. A simulation tool for analysis and design of reverse electrodialysis using concentrated brines. Chem. Eng. Res. Des. 93, 441–456.

Tian X.-l, Song S.-W., Chen F., Qi X.-J., Wang Y., Zhang Q.-H. Machine learning-guided property prediction of energetic materials: Recent advances, challenges, and perspectives. Energetic Materials Frontiers. 2022.

Tong, X., Liu, S., Yan, J., Broesicke, O.A., Chen, Y., Crittenden, J., 2020. Thermolytic osmotic heat engine for low-grade heat harvesting: thermodynamic investigation and potential application exploration. Appl. Energy 259, 114192.

Vasta, S., Freni, A., Sapienza, A., Costa, F., Restuccia, G., 2012. Development and lab-test of a mobile adsorption air-conditioner. Int. J. Refrig. 35 (3), 701–708.

Wu, J.W., Biggs, M.J., Hu, E.J., 2010. Thermodynamic analysis of an adsorption-based desalination cycle. Chem. Eng. Res. Des. 88 (12), 1541–1547.

Wu, J.W., Hu, E.J., Biggs, M.J., 2012. Thermodynamic cycles of adsorption desalination system. Appl. Energy 90 (1), 316–322.

Yip, N.Y., Elimelech, M., 2012. Thermodynamic and energy efficiency analysis of power generation from natural salinity gradients by pressure retarded osmosis. Environ. Sci. Technol. 46 (9), 5230–5239.

Zaragoza, G., Ruiz-Aguirre, A., Guillén-Burrieza, E., 2014. Efficiency in the use of solar thermal energy of small membrane desalination systems for decentralized water production. Appl. Energy 130, 491–499.

Zhao, Y., Luo, Z., Long, R., Liu, Z., Liu, W., 2020a. Performance evaluations of an adsorption-based power and cooling cogeneration system under different operative conditions and working fluids. Energy 204, 117993.

Zhao, Y., Li, M., Long, R., Liu, Z., Liu, W., 2020b. Dynamic modelling and analysis of an adsorption-based power and cooling cogeneration system. Energy Convers. Manag. 222, 113229.

Zhao, Y., Li, M., Long, R., Liu, Z., Liu, W., 2021. Dynamic modeling and analysis of an advanced adsorption-based osmotic heat engines to harvest solar energy. Renew. Energy 175, 638–649.